Solar Physics (2024) 299:101
https://doi.org/10.1007/s11207-024-02342-7

RESEARCH

Magnetic Imbalance at Supergranular Scale: A Driving Mechanism for Coronal Hole Formation

M. Cantoresi[1,2] **· F. Berrilli**[1]

Received: 8 February 2024 / Accepted: 20 June 2024 / Published online: 22 July 2024

Abstract
Unraveling the intricate interplay between the solar photosphere's magnetic field and the dynamics of the upper solar atmosphere is paramount to understanding the organization of solar magnetic fields and their influence on space weather events. This study delves into the organization of photospheric magnetic fields particularly in the context of coronal holes (CHs), as they are believed to harbor the sources of fast solar wind. We employed the signed measure technique on synthetic images that depict various arrangements of magnetic fields, encompassing imbalances in the sign of the magnetic field (inward and outward) and spatial organization.

This study provides compelling evidence that the cancellation functions of simulated regions with imbalanced magnetic fields along the boundaries of supergranular cells align with cancellation function trends of observed photospheric magnetic regions associated with CHs. Thus the analysis serves as a significant proof that CHs arise from the formation of imbalanced magnetic patterns on the edges of supergranular cells.

Keywords Coronal holes · Corona, quiet · Magnetic fields, photosphere

1. Introduction

The continuous emergence and evolution of magnetic fields within the photosphere (e.g., Viticchié et al. 2009; Archontis and Syntelis 2019) dictate the dynamics of the solar upper atmosphere (e.g., Trujillo Bueno and del Pino Alemán 2022), defining the overall architecture of the coronal magnetic field (e.g., Mikić et al. 1999). The solar surface's magnetic field exhibits a multiscale pattern, incorporating global-scale flows due to differential rotation and meridional circulation (e.g., Mackay and Yeates 2012; Obridko et al. 2021), and

✉ F. Berrilli
francesco.berrilli@roma2.infn.it

M. Cantoresi
cantoresi.1668918@studenti.uniroma1.it

1 Dipartimento di Fisica, Università degli Studi di Roma Tor Vergata, Viale Ricerca Scientifica 1, I-00133, Rome, Italy

2 Dipartimento di Fisica, Università degli Studi di Roma Sapienza, Piazzale Aldo Moro 5, I-00185, Rome, Italy

encompassing multiscale plasma flows generated by turbulent convection (e.g., Uritsky and Davila 2012; Berrilli, Scardigli, and Giordano 2013; Berrilli, Scardigli, and Del Moro 2014; Scardigli et al. 2021).

The continuous reconfiguration of the coronal magnetic field topology by these dynamic processes sets the stage for space weather events, including magnetic instabilities that trigger solar flares and coronal mass ejections (CMEs), as well as the high-speed solar wind streams. Notably, the high-speed solar wind is primarily sourced from CHs, as first observed by Krieger, Timothy, and Roelof (1973). CHs are distinct regions of the solar corona characterized by abnormally low density and temperature appearing as dark features in extreme ultraviolet (EUV) and soft X-ray (SXR) observations of the solar disk or limb, as described for the first time by Vaiana, Krieger, and Timothy (1973) and Vaiana et al. (1973).

One key distinguishing feature of CHs is the prevalence of a single magnetic polarity, suggesting an uneven distribution of magnetic flux (e.g., Cranmer 2009; Wang 2009). This dominance of magnetic polarity results in magnetic field lines that appear to extend far into interplanetary space rather than closing in the proximity of the Sun. Consequently, these field lines are often referred to as "open magnetic field lines." High-speed solar wind streams, formed from plasma that escapes the Sun's atmosphere due to the open magnetic field topology, flow freely through interplanetary space, impacting the surrounding environment, including the Earth's magnetosphere (e.g., McKenzie, Axford, and Banaszkiewicz 1997; Hofmeister et al. 2022). Despite the well-established connection between CHs and high-speed solar wind, the precise mechanisms behind CH formation and the predominant scales at which the imbalanced magnetic field organizes remain enigmatic and not definitively proven.

A model proposed by Fisk (2005) suggests that CHs form in regions with a reduced emergence rate of magnetic bipoles compared to quiet Sun (QS) regions, leading to the accumulation of open magnetic flux through interchange reconnection. Whereas Karachik, Pevtsov, and Abramenko (2010) proposed that CHs may originate from magnetic fields associated with decaying active regions, Hofmeister et al. (2017) conducted a statistical analysis of CHs and found that the imbalanced magnetic flux that characterizes CHs originates from small regions of the photosphere.

More recently, Hofmeister et al. (2019) studied the lifetimes of magnetic elements in 98 CHs and classified them into four categories based on their average lifetimes: associated with granulation, mesogranulation, supergranulation, and long-lived elements. The study revealed that a substantial portion, approximately 68%, of the magnetic flux imbalance in CHs is attributed to long-lived magnetic elements that exhibit no evident association with convective timescales.

In our recent study (Cantoresi, Berrilli, and Lepreti (2023), hereafter CBL), we performed a statistical analysis of line-of-sight (LoS) photospheric magnetic fields for 60 regions associated with CHs and 60 regions not associated with CHs (NCHs). We investigated the characteristics of the photospheric magnetic field distribution and the scaling relationships of spatial fluctuations in magnetic field polarity, deriving cancellation functions for all scenarios. The theory of signed measure uses "cancellation" to describe the condition where positive and negative contributions from a signal negate each other. This condition applies in situations like the spatial variations in the photospheric magnetic field, where opposing polarities can cancel out.

Our results revealed significant differences in the magnetic field properties between the two types of regions. Indeed, the cancellation functions calculated for the CH-associated regions differ from the cancellation functions of the non-CH regions; in the case of the CHs, we found that the cancellation exponent is generally lower compared to the NCHs regions.

Moreover, CH-associated regions show a plateau starting at supergranular scales (i.e., about 30 Mm). This suggests that CHs are characterized by a more sign-organized and amplified magnetic field configuration.

To validate or disprove this hypothesis, we conducted a series of simulations. We employed synthetic magnetograms, which represent different photospheric magnetic field patterns. These simulations cover regions with strong magnetic imbalance (coronal holes) and balanced regions (noncoronal holes) along supergranular boundaries. By analyzing these simulations, we can see how a specific technique (signed measure analysis) works under controlled conditions. Indeed, we calculated the average cancellation functions for these simulated patterns and compared them to the observed data. This analysis allows us to evaluate the results discussed in the CBL paper. By comparing these results to the data obtained from our supervised simulations we were able to validate the interpretation discussed in CBL paper.

The method used, the model to mimic different photospheric magnetic field distributions (associated to CH and NCH regions), and the analysis of the results are described in the next sections of the paper.

2. Data and Methods

2.1. The Singular Sign Measure

Photospheric magnetograms, when observed along the line-of-sight (LoS), exhibit fluctuations in flux orientation, which can be classified as outward (positive) and inward (negative) patterns, occurring both spatially and temporally. By scrutinizing solely the spatial variations in positive and negative magnetic flux across distinct scales we can discern a form of singularity embedded within photospheric magnetic fields. This property, known as sign singularity, forms the basis of the sign-singular measure theory (Zhai, Sreenivasan, and Yeung 2019).

Initially introduced by Ott et al. (1992) and applied to the multiscale measurement of the solar magnetic field by Ruzmaikin, Lawrence, and Cadavid (1993), this technique has since been utilized to characterize the complexity and multiscale properties of solar and heliophysical magnetism (e.g., Cadavid et al. 1994; Carbone and Bruno 1997; Consolini and Lui 1999; Sorriso-Valvo et al. 2003, 2015; Consolini et al. 2021; Cantoresi, Berrilli, and Lepreti 2023). The signed measure (e.g., Ott et al. 1992; Sorriso-Valvo et al. 2015) of a field $f(\mathbf{r})$ can be defined on a d-dimensional domain $Q(L)$ of size L. Let $Q_i(l) \subset Q(L)$ represent a partition of $Q(L)$ into disjoint subsets of size l. Then, for each scale l and for each disjoint set of boxes $Q_i(l)$, the signed measure is given by

$$\mu_i(l) = \frac{\int_{Q_i(l)} f(\mathbf{r}) d\mathbf{r}}{\int_{Q(L)} |f(\mathbf{r})| d\mathbf{r}}. \tag{1}$$

Generally, when the subset $Q_i(l)$ grows in size, the positive and negative magnetic components within each box tend to counteract each other, leading to a negligible impact on the signed measure. As the boxes get smaller and approach the typical size of the imbalanced magnetic structures, each box is more likely to contain a single sign-defined structure, reducing the level of cancellations. This process can be statistically characterized through the cancellation function

$$\chi(l) = \sum_{Q_i(l)} |\mu_i(l)|. \tag{2}$$

This function provides information about the sign of the field fluctuations. Indeed, the sign singular measure is a measure of the complexity of a magnetic field. It is considered sign singular if it changes sign at arbitrarily small scales. For magnetic fields that exhibit self-similarity, meaning that they have the same structure at different scales, Equation 2 follows a power law (Lawrence, Ruzmaikin, and Cadavid 1993). This means that the sign singular measure scales with the inverse of the scale of the field (Lawrence, Ruzmaikin, and Cadavid 1993):

$$\chi(l) \propto l^{-k}. \tag{3}$$

The cancellation index, denoted by the power law index k, is a quantitative measure of the efficiency of field cancellations in CH magnetic fields. It is calculated by plotting the cancellation function, which represents the fraction of photospheric magnetic flux that has canceled at each size scale, on a log-log scale. The slope of this plot provides the cancellation exponent k.

A higher value of k indicates more efficient field cancellations, with smaller scales being more likely to cancel than larger scales. A completely smooth field does not exhibit sign singularities, resulting in a cancellation index value of $k = 0$. In contrast, a Brownian noise field possesses a strong singularity, leading to a cancellation index value of $k = 1$. As previously reported, within the framework of signed measure theory, "field cancellation" refers to the specific spatial scale where the photospheric magnetic flux achieves a zero net value. This occurs due to the opposing polarities (positive and negative) balancing each other out.

2.2. Methods

In CBL, we identified regions of interest (RoIs) associated with CHs as the largest squares that could be inscribed within their boundaries. We extracted CH boundaries from SDO/Atmospheric Imaging Assembly (AIA) images and projected them onto SDO/HMI line-of-sight (LoS) magnetograms. CHs were segmented using the Spatial Possibilistic Clustering Algorithm (SPoCA) (Verbeeck et al. 2014), which employs fuzzy clustering for CH extraction. We remember that SDO/HMI Doppler camera observes the Zeeman splitting of photospheric Fe I ions at 6173.3 Å. The data product contains low-cadence, low-noise magnetograms at a plate scale of 0.505 arcsec pixel^{-1} and a photon noise level of 5 G near the disk center (Couvidat et al. 2016; Hofmeister et al. 2017). CH regions were identified in magnetograms spanning from 2013 to 2019 (maximum and descending phase of SC-24), whereas quiet Sun regions (NCHs) were chosen during the period of minimum between SC-24 and SC-25 to mitigate the influence of magnetic active regions. NCH RoIs were chosen from quiet Sun areas, ensuring their dimensions matched those of the CH RoIs. All these regions were selected near the center of the solar disk (within $\pm 30^\circ$ of heliographic latitude and longitude) to minimize projection effects. Additionally, the heliographic angle was computed for all pixels in the magnetogram to derive radial magnetic fields from LoS fields. We derived the cancellation functions for these regions using Equations 1 and 2. By primarily focusing on the cancellation indices obtained by fitting Equation 3 with a power law, we compared the properties of the cancellation functions of the two classes of events, CH and NCH. Furthermore, we investigated the spatial scales over which the magnetic field's polarity changes from singular to smooth (i.e., when $k = 0$).

As previously mentioned, CBL main findings, based on the sign-singularity analysis of HMI magnetograms, demonstrate that the magnetic field imbalance in CHs primarily arises from the supergranular scale (approximately 30 Mm). This result strongly corroborates the

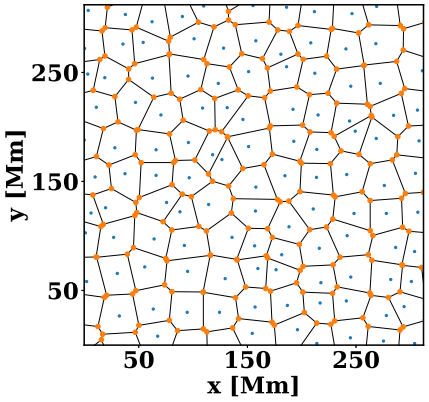

Figure 1 Example of a Voronoi network (black lines) superimposed on the blue points, which represent the generator points. Orange points represent the vertices of the supergranular network.

hypothesis that CHs originate from the organization of magnetic fields of a specific polarity along the edges of supergranular structures. We refer the reader to the CBL paper for more detail. In this study, we employed a similar approach, but with synthetic photospheric regions to simulate completely imbalanced photospheric regions (CHs), quiet Sun regions (NCHs), and intermediate scenarios, to interpret the results reported in CBL.

The region of interest (RoI) depicted in the simulations is represented by a 840×840 square pixels matrix, which corresponds to an area of approximately 310 square megameters based on the HMI plate scale. To simulate the intensity of the ubiquitous magnetic fields in the solar photosphere, we selected values from a standardized Gaussian distribution with a standard deviation of 1σ. Subsequently, we simulated the supergranular network using a Voronoi tessellation, which is an adaptable geometrical model that aptly represents such solar web-like spatial patterns (e.g., Schrijver, Hagenaar, and Title 1997; Berrilli et al. 1999; De Rosa and Toomre 2004; Caroli et al. 2015; Del Moro et al. 2015). This tessellation, able to partition the plane into distinct regions, assigns points based on their proximity to a set of seed points. Each point belongs to the region associated with the nearest seed point, ensuring that no other seed point is closer. This can be visualized as a set of invisible fences around each seed point, with each point residing in the region of the closest fence. To generate these regions, we utilized a pattern approach, as described in previous papers such as Berrilli, Scardigli, and Del Moro (2014).

The Voronoi region $V(p)$ associated with a generator point p in the set of generator points P is described by the equation

$$V(p) = \left\{ x \in \mathbb{R}^2 \mid \|x - p\| \leq \|x - q\| \; \forall q \in P, q \neq p \right\}, \tag{4}$$

where the variable x represents a point in the plane, and q and p are two generator points. The equation states that a point x belongs to the Voronoi region $V(p)$ if the distance between x and p is less than or equal to the distance between x and any other generator point q in P, where q is not equal to p. For more information about Voronoi tessellation, we refer to Watson (1993).

We deployed the generator points across the domain in a regular pattern resembling crystal geometry in such a way that the first nearest-neighbor distance corresponds to the supergranular linear scale. These points were then perturbed with a random displacement derived from a Gaussian distribution, and the Voronoi pattern (see Figure 1) was derived from Equation 4. To replicate the characteristics of CH and NCH magnetograms, we utilize magnetic patches segmented in an SDO/HMI line-of-sight magnetogram. The magnetic flux

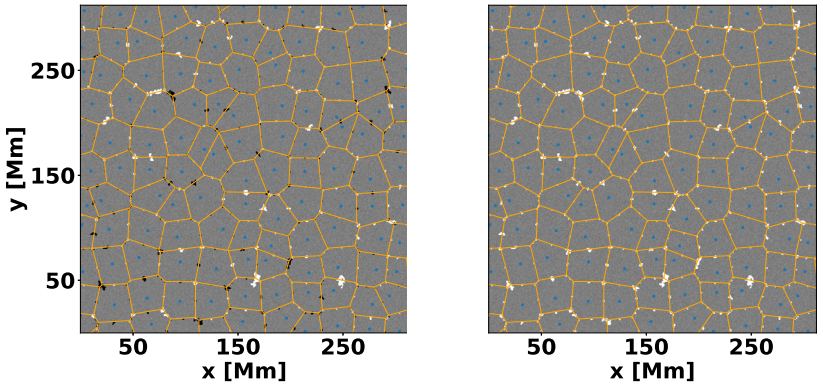

Figure 2 Examples of RoI simulations for the NCHs balanced (left panel) and CHs imbalanced (right panel) photospheric magnetic field, with the Voronoi diagram (orange skeleton) overplotted. Positive magnetic elements are shown in white, whereas negative magnetic elements are shown in black. The blue points represent the seeds used to generate the skeleton of the Voronoi diagram. The images have been saturated at ± 10 G.

patches that shape our Voronoi network were derived from the magnetogram acquired on 27 November 2019, at 00:00 UTC. Identifying pixels with magnetic field density greater than 3σ above the noise level (designated by σ) in the magnetogram allowed for the segmentation of magnetic patches or elements.

The segmented magnetic elements were positioned within the simulation domain such that their centroids coincided with the vertices of the Voronoi diagram, and an additional midpoint was placed at the center of each vertex (see Figure 2). We defined three simulation setups to simulate three different types of network magnetic field configurations: imbalanced (CHs), balanced (NCHs), and partially imbalanced (or intermediate) magnetic field (see Figure 2). In the completely imbalanced case, network magnetic elements have all the same polarity; in the completely balanced case, the polarity is randomly defined. To explore the scenario that falls between two extremes, i) completely imbalanced, i.e., all magnetic elements have the same polarity, and ii) completely balanced, i.e., the total magnetic flux within a defined area is zero (equal amounts of north and south polarity), we simulate an intermediate case with partial imbalance. In this case, one magnetic polarity is dominant, but not completely overwhelming; in particular, the probability that a magnetic element within the simulation domain has a specific polarity is approximately 70%.

For each of the three cases, we performed 1000 repetitions of the simulations and calculated the cancellation function per each. In each simulation, different Voronoi diagrams were generated with different positions of the magnetic elements. In our study CBL, we compared the distribution of cancellation exponents k for selected CHs to the distribution of k for NCHs, finding that the sign of the magnetic field is more singular in the case of NCHs. In this study, we estimated the slope of the curves by calculating the numerical derivatives of the synthetic cancellation functions. This approach allowed us to assess the efficiency of magnetic field cancellation at specific scales. We calculated the numerical derivatives for all estimated $\chi(l)$ values and presented their means in Figure 3. The error was determined by calculating the standard deviation of the ensemble.

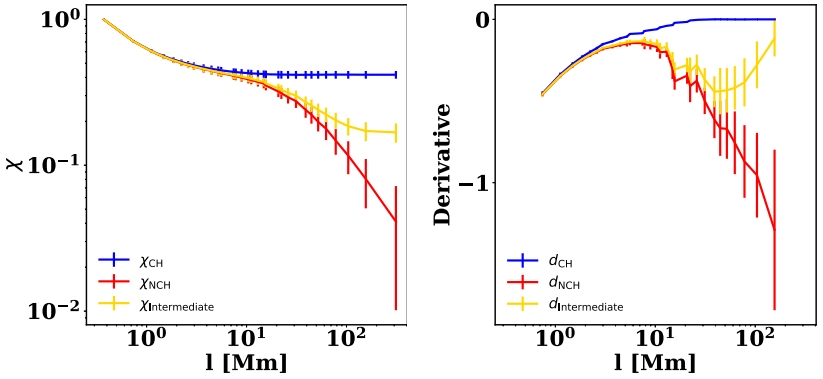

Figure 3 The figures show the cancellation functions (left panel) and their numerical derivatives (right panel) for the CHs imbalanced (blue), NCHs completely balanced (red), and intermediate (yellow) cases. The confidence interval is 1σ.

3. Results and Discussion

In this work, we have used the cancellation analysis to study different organization of simulated photospheric magnetic fields. The results are mainly summarized in Figure 3: in the panel in the left, we report the cancellation functions for the considered cases (in blue, red, and yellow, respectively, the imbalanced, balanced, and slightly imbalanced network fields); on the right the same for the numerical derivatives. The plots reveal minimal discrepancy between cancellation functions and derivatives at small scales (around 10 Mm), diverging primarily at larger scales. On the largest scales, for the RoIs with imbalanced fields, the derivative of the cancellation functions is almost zero, meaning that there is no more cancellation, i.e., the magnetic field is smooth (Ott et al. 1992).

Conversely, for the RoIs with balanced fields, the derivative exhibits a contrary behavior, attaining its maximum value at around 10 Mm and then declining. The slightly imbalanced case exhibits an intermediate behaviour: the derivative falls, then rises toward zero, mimicking the imbalanced scenario. All these trends become clear when considering Equation 1. If we evaluate the integral over small scales (smaller than the average distance between magnetic elements of the network), the dominant contribution to the cancellation function (and therefore the sign singularity of the field) mainly arises from the intermittent Gaussian fields, representing the small-scale magnetic components. At distances comparable to the separation between individual magnetic elements, the overall signal becomes dominated by the larger-scale magnetic pattern. This leads to a divergence in the behavior of the three individual trends in Figure 3. This divergence in the trends is particularly visible from the supergranular scale, where the cancellation function for the imbalanced case becomes constant (the derivative null). On the supergranular scale the singularity of the sign of the field is dominated by the large-scale magnetic pattern, causing nearly all integration boxes to reflect the field sign dictated by the magnetic network.

Our simulations successfully reproduce the qualitative behavior of the cancellation functions measured in CLB. This can be seen in Figure 4, where the reported example of cancellation functions for real magnetograms closely resemble those derived from the analysis of the simulated magnetic field in Figure 3.

Notably, the simulated imbalanced cases closely resemble the CHs. As reported in CLB, 83% of the cancellation functions in analyzed CHs display a plateau triggered at an average

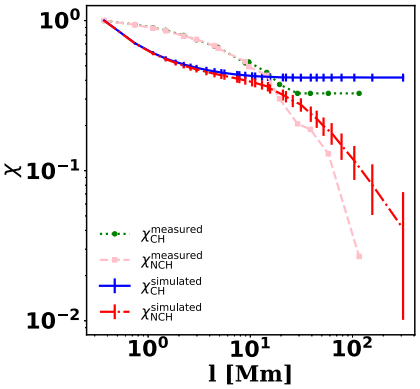

Figure 4 The figure displays estimated cancellation functions for both CH (green circles) and NCH (pink squares), as published in CLB, together with the simulated cancellation functions shown in the left panel of Figure 3 (solid blue line shows the CH, dash-dot red line the NCH case). Whereas the CH and NCH functions (both measured and simulated) closely resemble each other at smaller scales, a clear divergence emerges for larger scales. Additionally, a distinct plateau is visible for the CH cancellation functions at the supergranular scale.

linear scale of 36 ± 12 Mm, which corresponds roughly to the supergranulation. Our investigations with simulated, highly imbalanced magnetic fields yielded a consistent observation: in examined cases the plateau begins at a distance of 27 ± 2 Mm. This value closely matches the average distance at which we placed the generators within the Voronoi diagram, which serves to simulate the supergranular magnetic fields. The reported value of the scale in which the plateau is triggered is an average of the scales estimated per all the cancellation functions. To determine the points on the plateau, we computed the numerical derivative of the cancellation function, following the same procedure described in CLB. The plateau is then identified by all the points with a numerical derivative below a specified threshold. The scale in which the plateau initiates is estimated by averaging the first point of the plateau with the previous one. The value chosen for the threshold is of 10^{-4}, following the methodology outlined in CLB. This study further strengthens the conclusion reached in CLB, demonstrating that the imbalance in photospheric magnetic fields within CHs is predominantly confined to the supergranular scale marked by the magnetic network.

To conclude this section, we examine the roles of two parameters in the simulations: i) the level of fluctuation in the magnetic noise (represented by the standard deviation σ of the Gaussian distribution of magnetic element intensities) and ii) the variance of the probability distribution controlling the shifts in the centers of the Voronoi diagram generators.

In our simulations, we mimic small-scale magnetic elements by setting the standard deviation at the value 1σ. We investigate how the selection of a 1σ value affects cancellation functions. We achieve this by calculating these functions for simulated CHs using a range of standard deviation values around this value. Consistent with our expectations, the impact on cancellation functions is primarily observed at smaller spatial scales. With increasing σ, the calculated cancellation functions exhibit a convergence to a purely Gaussian behavior. A variation in the amplitude of the intermittent magnetic field leads to changes in the cancellation index k. As discussed in Section 2 and by other authors (e.g., Consolini et al. 1999), as σ increases, k tends to its limit value of 1. The slope of the cancellation functions remains consistent across larger scales, regardless of the specific value chosen for σ. This suggests that our findings are not significantly affected by the choice of a realist value for σ, particularly at supergranular scales.

The second parameter governs the displacements of the Voronoi diagram's generator center. To create a pattern resembling the Sun's surface, we placed the generators in a uniform grid, then randomly shifted them based on a normal distribution with a standard deviation of 15σ. This value aims to capture the variations observed in the sizes of solar supergranular cells (e.g., Berrilli et al. 2004). Decreasing the σ value in the Voronoi diagram makes it resemble a regular lattice, whereas increasing σ leads to a more disordered pattern. However, within a realistic range of σ values, the chosen value has negligible impact on the estimated scale of organization.

4. Conclusions

In CLB, we examined physical properties of the photospheric magnetic field of various solar regions. These regions included both CHs (areas with open magnetic field lines) and NCH regions (areas with closed magnetic field lines, representing relatively undisturbed parts of the Sun's atmosphere).

Analyzing the properties of the distributions of the magnetic fields in these regions, we reported that the magnetic field in CH regions is less balanced compared to NCH magnetic fields, confirming what is reported in the current literature (as mentioned in Section 1). Our investigation went beyond simply verifying the imbalance. By applying the signed measure technique we were able to measure the characteristic scale at which it occurs. Our analysis revealed that this imbalance becomes evident at the supergranular scale. Based on our analysis, we speculate about the organization of CHs' photospheric magnetic fields. We hypothesize that the magnetic network, linked to supergranular cells, exhibits an imbalance in the arrangement of magnetic elements, dependent on the magnetic polarity.

To validate the hypothesis from CLB, we simulated various magnetic imbalance conditions arranged on a pattern derived from the Voronoi algorithm. This algorithm is designed to replicate the magnetic network structure observed in supergranular cells. We simulated three types of magnetic field configurations, imbalanced (CHs), balanced (NCHs), and mixed, and calculated their associated cancellation functions. Comparing these to those observed in real CHs and NCHs, we found consistent behavior. Notably, the simulated cancellation function trends diverged primarily at supergranular scales, mirroring the pattern observed in the real data and reported in CLB.

Our findings suggest that the magnetic field loses its singularity at supergranular scales. This is further confirmed by analyzing simulated CHs, which reveals that the scale at which the field sign becomes smooth coincides with the average distance between the points generating the Voronoi diagram (generator points in Equation 4).

This finding strongly supports the hypothesis that the footpoints of coronal funnels in CHs (representing open coronal magnetic fields) are primarily located at the supergranular network, consistent with current literature (i.e., Hofmeister et al. (2017), Hofmeister et al. (2019), Tu et al. (2005)). Recent studies using Parker Solar Probe data (Bale et al. 2021, 2023) identified microstreams in the solar wind originating from CHs. These microstreams display angular scales comparable to supergranular cells. These results further strengthen our previous conclusion that the photospheric magnetic fields within CHs are not uniformly distributed. Instead, they show an imbalance that mirrors the pattern of the magnetic network associated with supergranular cells.

The observed link between supergranulation and coronal holes suggests that advective plasma flows associated with supergranulation may play a significant role in the formation and organization of unbalanced magnetic patches. These patches are thought to be remnants

of decayed active regions, and they potentially contribute to the formation of isolated coronal holes at active latitudes (e.g., Harvey and Recely 2002; Karachik, Pevtsov, and Abramenko 2010). This study underlines the importance of two key approaches for studying coronal hole (CH) formation in the era of advanced space weather instruments: 1) creating realistic simulations using forward modeling to compare with observations and 2) analyzing both simulations and observations with the same tools. This framework, based on magnetic network simulations, offers a valuable tool for understanding CH formation.

Acknowledgments This paper is partially based on Master's thesis research "Cancellation properties in quiet-Sun photosphere hosting Coronal Holes and ephemeral regions" conducted by M.C. under the supervision of Prof. F. Berrilli. M.C. was supported by the Joint Research PhD Program in Astronomy, Astrophysics, and Space Science between the universities of Roma Tor Vergata, Roma Sapienza, and INAF. This research has been carried out in the framework of the CAESAR (Comprehensive spAce wEather Studies for the ASPIS prototype Realization) project, supported by the Italian Space Agency and the National Institute of Astrophysics through the ASI-INAF n.2020-35-HH.0 agreement for the development of the ASPIS (ASI SPace weather InfraStructure) prototype of scientific data center for Space Weather.

Author contributions F.B. and M.C. planned and discussed the analysis, performed by M.C. Both M.C. and F.B. wrote the main manuscript text. M.C. prepared the figures. All authors reviewed the manuscript.

Funding Open access funding provided by Università degli Studi di Roma Tor Vergata within the CRUI-CARE Agreement.

Data Availability Data used for the analysis (the magnetogram from HMI/SDO) are available at the website of the JSOC: http://jsoc.stanford.edu/ajax/exportdata.html

Declarations

Competing interests The authors declare no competing interests.

References

Archontis, V., Syntelis, P.: 2019, The emergence of magnetic flux and its role on the onset of solar dynamic events. *Phil. Trans. Roy. Soc. London Ser. A, Math. Phys. Sci.* **377**, 20180387. DOI. ADS.

Bale, S.D., Horbury, T.S., Velli, M., Desai, M.I., Halekas, J.S., McManus, M.D., Panasenco, O., Badman, S.T., Bowen, T.A., Chandran, B.D.G., Drake, J.F., Kasper, J.C., Laker, R., Mallet, A., Matteini, L., Phan, T.D., Raouafi, N.E., Squire, J., Woodham, L.D., Woolley, T.: 2021, A solar source of Alfvénic magnetic field switchbacks: in situ remnants of magnetic funnels on supergranulation scales. *Astrophys. J.* **923**, 174. DOI. ADS.

Bale, S.D., Drake, J.F., McManus, M.D., Desai, M.I., Badman, S.T., Larson, D.E., Swisdak, M., Horbury, T.S., Raouafi, N.E., Phan, T., Velli, M., McComas, D.J., Cohen, C.M.S., Mitchell, D., Panasenco, O., Kasper, J.C.: 2023, Interchange reconnection as the source of the fast solar wind within coronal holes. *Nature* **618**, 252. DOI. ADS.

Berrilli, F., Scardigli, S., Del Moro, D.: 2014, Magnetic pattern at supergranulation scale: the void size distribution. *Astron. Astrophys.* **568**, A102. DOI. ADS.

Berrilli, F., Scardigli, S., Giordano, S.: 2013, Multiscale magnetic underdense regions on the solar surface: granular and mesogranular scales. *Solar Phys.* **282**, 379. DOI. ADS.

Berrilli, F., Ermolli, I., Florio, A., Pietropaolo, E.: 1999, Average properties and temporal variations of the geometry of solar network cells. *Astron. Astrophys.* **344**, 965. ADS.
Berrilli, F., Del Moro, D., Consolini, G., Pietropaolo, E., Duvall, J.T.L., Kosovichev, A.G.: 2004, Structure properties of supergranulation and granulation. *Solar Phys.* **221**, 33. DOI. ADS.
Cadavid, A., Lawrence, J., Ruzmaikin, A., Kayleng-Knight, A.: 1994, Multifractal models of small-scale solar magnetic fields. *Astrophys. J.* **429**, 391.
Cantoresi, M., Berrilli, F., Lepreti, F.: 2023, Organization scale of photospheric magnetic imbalance in coronal holes. *Atti Accad. Naz. Lincei, Rend. Cl. Sci. Fis. Mat. Nat.*. DOI. ADS.
Carbone, V., Bruno, R.: 1997, Sign singularity of the magnetic helicity from in situ solar wind observations. *Astrophys. J.* **488**, 482. DOI.
Caroli, A., Giannattasio, F., Fanfoni, M., Del Moro, D., Consolini, G., Berrilli, F.: 2015, Turbulent convective flows in the solar photospheric plasma. *J. Plasma Phys.* **81**, 495810514. DOI. ADS.
Consolini, G., Lui, A.T.Y.: 1999, Sign-singularity analysis of current disruption. *Geophys. Res. Lett.* **26**, 1673. DOI. ADS.
Consolini, G., Carbone, V., Berrilli, F., Bruno, R., Bavassano, B., Briand, C., Caccin, B., Ceppatelli, G., Egidi, A., Ermolli, I., Florio, A., Mainella, G., Pietropaolo, E.: 1999, Scaling behavior of the vertical velocity field in the solar photosphere. *Astron. Astrophys.* **344**, L33. ADS.
Consolini, G., De Michelis, P., Coco, I., Alberti, T., Marcucci, M.F., Giannattasio, F., Tozzi, R.: 2021, Sign-singularity analysis of field-aligned currents in the ionosphere. *Atmosphere* **12**, 708. DOI. https://www.mdpi.com/2073-4433/12/6/708.
Couvidat, S., Schou, J., Hoeksema, J.T., Bogart, R.S., Bush, R.I., Duvall, T.L., Liu, Y., Norton, A.A., Scherrer, P.H.: 2016, Observables processing for the helioseismic and magnetic imager instrument on the solar dynamics observatory. *Solar Phys.* **291**, 1887. DOI. ADS.
Cranmer, S.R.: 2009, Coronal holes. *Living Rev. Solar Phys.* **6**, 3. DOI. ADS.
De Rosa, M.L., Toomre, J.: 2004, Evolution of solar supergranulation. *Astrophys. J.* **616**, 1242. DOI. ADS.
Del Moro, D., Giannattasio, F., Berrilli, F., Consolini, G., Lepreti, F., Gošić, M.: 2015, Super-diffusion versus competitive advection: a simulation. *Astron. Astrophys.* **576**, A47. DOI. ADS.
Fisk, L.A.: 2005, The open magnetic flux of the Sun. I. transport by reconnections with coronal loops. *Astrophys. J.* **626**, 563. DOI. ADS.
Harvey, K.L., Recely, F.: 2002, Polar coronal holes during cycles 22 and 23. *Solar Phys.* **211**, 31. DOI. ADS.
Hofmeister, S.J., Veronig, A., Reiss, M.A., Temmer, M., Vennerstrom, S., Vršnak, B., Heber, B.: 2017, Characteristics of low-latitude coronal holes near the maximum of solar cycle 24. *Astrophys. J.* **835**, 268. DOI. ADS.
Hofmeister, S.J., Utz, D., Heinemann, S.G., Veronig, A., Temmer, M.: 2019, Photospheric magnetic structure of coronal holes. *Astron. Astrophys.* **629**, A22. DOI. ADS.
Hofmeister, S.J., Asvestari, E., Guo, J., Heidrich-Meisner, V., Heinemann, S.G., Magdalenic, J., Poedts, S., Samara, E., Temmer, M., Vennerstrom, S., Veronig, A., Vršnak, B., Wimmer-Schweingruber, R.: 2022, How the area of solar coronal holes affects the properties of high-speed solar wind streams near Earth: an analytical model. *Astron. Astrophys.* **659**, A190. DOI. ADS.
Karachik, N., Pevtsov, A., Abramenko, V.: 2010, Formation of coronal holes on the ashes of active regions. In: *Astronomical Society Meeting Abstracts #216*. 401.04. ADS.
Krieger, A.S., Timothy, A.F., Roelof, E.C.: 1973, A coronal hole and its identification as the source of a high velocity solar wind stream. *Solar Phys.* **29**, 505. DOI. ADS.
Lawrence, J.K., Ruzmaikin, A.A., Cadavid, A.C.: 1993, Multifractal measure of the solar magnetic field. *Astrophys. J.* **417**, 805. DOI. ADS.
Mackay, D.H., Yeates, A.R.: 2012, The Sun's global photospheric and coronal magnetic fields: observations and models. *Living Rev. Solar Phys.* **9**, 6. DOI. ADS.
McKenzie, J.F., Axford, W.I., Banaszkiewicz, M.: 1997, The fast solar wind. *Geophys. Res. Lett.* **24**, 2877. DOI. ADS.
Mikić, Z., Linker, J.A., Schnack, D.D., Lionello, R., Tarditi, A.: 1999, Magnetohydrodynamic modeling of the global solar corona. *Phys. Plasmas* **6**, 2217. DOI. ADS.
Obridko, V.N., Pipin, V.V., Sokoloff, D., Shibalova, A.S.: 2021, Solar large-scale magnetic field and cycle patterns in solar dynamo. *Mon. Not. Roy. Astron. Soc.* **504**, 4990. DOI. ADS.
Ott, E., Du, Y., Sreenivasan, K.R., Juneja, A., Suri, A.K.: 1992, Sign-singular measures: fast magnetic dynamos, and high-Reynolds-number fluid turbulence. *Phys. Rev. Lett.* **69**, 2654. DOI. ADS.
Ruzmaikin, A.A., Lawrence, J.K., Cadavid, A.C.: 1993, Multiscale measure of the solar magnetic field. In: *Bulletin of the American Astronomical Society* **25**, 1219. ADS.
Scardigli, S., Berrilli, F., Del Moro, D., Giovannelli, L.: 2021, Stellar turbulent convection: the multiscale nature of the solar magnetic signature. *Atmosphere* **12**, 938. DOI. ADS.
Schrijver, C.J., Hagenaar, H.J., Title, A.M.: 1997, On the patterns of the solar granulation and supergranulation. *Astrophys. J.* **475**, 328. DOI. ADS.

Sorriso-Valvo, L., Abramenko, V., Carbone, V., Noullez, A., Politano, H., Pouquet, A., Veltri, P., Yurchyshyn, V.: 2003, Cancellations analysis of photospheric magnetic structures and flares. *Mem. Soc. Astron. Ital.* **74**, 631. ADS.

Sorriso-Valvo, L., De Vita, G., Kazachenko, M.D., Krucker, S., Primavera, L., Servidio, S., Vecchio, A., Welsch, B.T., Fisher, G.H., Lepreti, F., Carbone, V.: 2015, Sign singularity and flares in solar active region NOAA 11158. *Astrophys. J.* **801**, 36. DOI. ADS.

Trujillo Bueno, J., del Pino Alemán, T.: 2022, Magnetic field diagnostics in the solar upper atmosphere. *Annu. Rev. Astron. Astrophys.* **60**, 415. DOI. ADS.

Tu, C.-Y., Zhou, C., Marsch, E., Xia, L.-D., Zhao, L., Wang, J.-X., Wilhelm, K.: 2005, Solar wind origin in coronal funnels. *Science* **308**, 519. DOI. ADS.

Uritsky, V.M., Davila, J.M.: 2012, Multiscale dynamics of solar magnetic structures. *Astrophys. J.* **748**, 60. DOI. ADS.

Vaiana, G.S., Krieger, A.S., Timothy, A.F.: 1973, Identification and analysis of structures in the corona from X-ray photography. *Solar Phys.* **32**, 81. DOI. ADS.

Vaiana, G.S., Davis, J.M., Giacconi, R., Krieger, A.S., Silk, J.K., Timothy, A.F., Zombeck, M.: 1973, X-ray observations of characteristic structures and time variations from the solar corona: preliminary results from SKYLAB. *Astrophys. J. Lett.* **185**, L47. DOI. ADS.

Verbeeck, C., Delouille, V., Mampaey, B., De Visscher, R.: 2014, The SPoCA-suite: software for extraction, characterization, and tracking of active regions and coronal holes on EUV images. *Astron. Astrophys.* **561**, A29. DOI. ADS.

Viticchié, B., Del Moro, D., Berrilli, F., Bellot Rubio, L., Tritschler, A.: 2009, Imaging spectropolarimetry with IBIS: evolution of bright points in the quiet Sun. *Astrophys. J. Lett.* **700**, L145. DOI. ADS.

Wang, Y.-M.: 2009, Coronal holes and open magnetic flux. *Space Sci. Rev.* **144**, 383. DOI. ADS.

Watson, D.: 1993, Spatial tessellations: concepts and applications of Voronoi diagrams. By Atsuyuki Okabe, Barry Boots, and Kokichi Sugihara, 1992, John Wiley & Sons, New York, 532 p., ISBN 0 471 93430 5, US $112.00. *Comput. Geosci.* **19**, 1209. DOI. ADS.

Zhai, X.M., Sreenivasan, K.R., Yeung, P.K.: 2019, Cancellation exponents in isotropic turbulence and magnetohydrodynamic turbulence. *Phys. Rev. E* **99**, 023102. DOI.